

Impact of root water content on root biomass estimation using ground penetrating radar: evidence from forward simulations and field controlled experiments

Li Guo · Henry Lin · Bihang Fan ·
Xihong Cui · Jin Chen

Received: 19 September 2012 / Accepted: 28 March 2013 / Published online: 18 April 2013
© Springer Science+Business Media Dordrecht 2013

Abstract

Background and aims The GPR indices used for predicting root biomass are measures of root radar reflectance. However, root radar reflectance is highly correlated with root water content. The objectives of this study are to assess the impact of root water content on GPR-based root biomass estimation and to develop more reliable approaches to quantify root biomass using GPR.

Methods Four hundred nine roots of five plant species in a sandy area of northern China were examined to determine the general water content range of roots in sandy soils. Two sets of GPR simulation scenarios (including 492 synthesized radargrams in total) were then conducted to compare the changes of root radar signal and the accuracies of root biomass estimation by GPR at different root gravimetric water content levels. In

the field, GPR transects were scanned for *Ulmus pumila* roots buried in sandy soils with three antenna center frequencies (0.5, 0.9, and 2.0 GHz). The performance of two new GPR-based root biomass quantification approaches (one using time interval GPR index and the other using a non-linear regression model) was then tested.

Results All studied roots exhibited a broad range of gravimetric water content (>125 %), with the water contents of most roots ranging from 90 % to 150 %. Both field experiments and forward simulations indicated that 1) waveforms of root radar reflection, radar-reflectance related GPR indices, and root biomass estimation accuracy were all affected by root water content; and 2) using time interval index and establishing a nonlinear regression model of root biomass on GPR indices improved the accuracy of root biomass estimation, decreasing the prediction error (*RMSE*) by 4 to 30 % under field conditions.

Conclusions The magnitude of GPR indices depends on both root biomass and root water content, and root water content affects root biomass estimation using GPR indices. Using a linear regression model of root biomass on radar-reflectance related GPR index for root biomass estimation would only be feasible for roots with a relative narrow range of water content (e.g., when gravimetric water contents of studied roots vary within 20 %). Appropriate GPR index and regression

Responsible Editor: Peter J. Gregory.

L. Guo · B. Fan · X. Cui · J. Chen (✉)
State Key Laboratory of Earth Surface Processes and
Resource Ecology, Beijing Normal University,
Beijing 100875, China
e-mail: chenjin@bnu.edu.cn

H. Lin
Department of Ecosystem Science and Management, The
Pennsylvania State University,
University Park, PA 16802, USA

models should be selected based on the water content range of roots. The new protocol of root biomass quantification by GPR presented in this study improves the accuracy of root biomass estimation.

Keywords Ground penetrating radar · Noninvasive root investigation · Root biomass estimation · Root water content · Forward simulation · Controlled field experiment

Abbreviations

GPR Ground penetrating radar
EM Electromagnetic
RMSE Root mean square error
LOOCV Leave-one-out cross validation

Introduction

As a non-destructive subsurface detection technique, ground penetrating radar (GPR) has been used in coarse root investigation since the end of last century (Hruška et al. 1999). Because of its unique advantages (including its non-destructive nature, ability for rapid data collection, and repeatable sampling through time) as compared to the traditional invasive methods for root biomass quantification (e.g., soil coring, uprooting, and excavation), GPR is becoming an alternative approach for in situ coarse root biomass estimation (Guo et al. 2013a).

Butnor et al. (2001) was the first to apply GPR for root biomass prediction, in which total root biomass (g/m^2) to the depth of 40 cm of loblolly pine (*Pinus taeda*) was correlated with root radar reflectance and root reflector counts on radargrams, respectively, although the correlation coefficients were relatively low ($r=0.34\sim 0.57$). With the aid of advanced GPR signal post-processing procedures (e.g., Kirchhoff migration and Hilbert transform), Butnor et al. (2003) greatly improved the correlation between root biomass from soil cores (g/core) and GPR reflectance ($r=0.86$). Based on the GPR data processing procedure presented in Butnor et al. (2003), several subsequent studies estimated root biomass using the statistical correlation between the strength of root radar reflectance and root biomass per core (e.g., Stover et al. 2007; Butnor et al. 2008) or root biomass per area (e.g., Samuelson et al. 2008) (Table 1). Cui et al. (2011) subsequently established a

strong correlation linking fresh weights (g) of roots to the corresponding time interval GPR index (Δt) through a field controlled experiment (Table 1). Most recently, Cui et al. (2012) correlated the biomass (g) and fresh weight (g) of single buried root with the strength of root radar reflectance (Table 1). In addition, Hirano et al. (2012) and Cui et al. (2011) used the correlation between root diameter and root biomass/fresh weight to indirectly predict root biomass and fresh weight from the root diameters estimated by GPR, respectively.

Root biomass estimation using GPR in several locations (e.g., southeastern U.S., northern China, and coastal of Japan) has shown that its performance is site-specific (Butnor et al. 2001; Hirano et al. 2012; Guo et al. 2013a). Soil conditions (e.g., soil water content, soil texture, and leaf litter layer) and root properties (especially root water content) significantly influence the accuracy of root detection and root biomass estimation using GPR (Butnor et al. 2001; Dannoura et al. 2008; Hirano et al. 2009; Guo et al. 2013a). However, the impact of root water content was seldom recognized in the previous studies (Hirano et al. 2009). Only Dannoura et al. (2008) found that the contrast in water content between root and soil was important for precise root delineation, and Hirano et al. (2009) confirmed that dried roots (with volumetric water content $<20\%$) could not be detected by GPR in a sandbox with soil volumetric water content of approximately 15 %.

According to electromagnetic (EM) theory, dielectric constant and electrical conductivity are the most crucial parameters that govern GPR signal propagation and reflection (Conyers 2004). Specifically, the contrast in dielectric constants between a root and the surrounding soil determines root radar reflectance (al Hagrey 2007):

$$R = \frac{\sqrt{\varepsilon_{r1}} - \sqrt{\varepsilon_{r2}}}{\sqrt{\varepsilon_{r1}} + \sqrt{\varepsilon_{r2}}}, \quad (1)$$

where R is the reflection coefficient (an indicator of the reflected energy amplitude with respect to the total signal amplitude), and ε_{r1} and ε_{r2} are the dielectric constants of root and soil, respectively. Electrical conductivity determines the percentage of radar energy that will be attenuated when propagating through a medium (Conyers 2004). Because of the high dielectric constant of water (81) compared to

Table 1 A summary of published studies on the estimation of root biomass or fresh weight using GPR, including plant species, soil conditions, GPR index used, antenna center frequency, sample size for correlation analysis, and the correlation coefficient between GPR index and root biomass or fresh weight

Species	Soil type	Soil texture		Soil drainage condition	GPR index used for root biomass or fresh weight estimation	Antenna frequency (GHz)	Sample size	Correlation coefficient (r)	Reference [†]
		Sand (%)	Clay and Silt (%)						
<i>Pinus taeda</i>	Wakulla soil	85~92	8~15	Well	Areas within threshold range	1.5	64 (16) ^a	0.34 (0.55) ^a	Butnor et al. 2001
<i>P. taeda</i>	Wakulla soil	85~92	8~15	Well	Reflector tally	1.5	64 (16) ^a	0.36 (0.49) ^a	Butnor et al. 2001
<i>P. taeda</i>	Troup and Lucy soil	> 70*	<30*	Well	Pixels within threshold range	1.5	60	0.86	Butnor et al. 2003
<i>Quercus sp.</i>	Sandy Pomello soil	> 90*	<10*	Well	Pixels within threshold range	1.5	30	0.88	Stover et al. 2007
<i>P. taeda</i> ,	Sandy soil	> 90*	<10*	Well	Pixels within threshold range	1.5	40	0.51, 0.80 ^b	Butnor et al. 2008
<i>Q. sp.</i>	Sandy Pomello soil	> 90*	<10*	Well	Pixels within threshold range	1.5	40	0.84, 0.82 ^b	Butnor et al. 2008
<i>P. taeda</i>	Grossarenic Paleodults	> 60*	<40*	Well	Pixels within threshold range	1.5	84	0.89	Samuelson et al. 2008
<i>Ulmus pumila</i>	Sandy soil	95	5	Well	Time interval	2.0	30	0.89 ^c	Cui et al. 2011
<i>U. Pumila</i>	Sandy soil	95	5	Well	High amplitude area	0.5	25	0.91, 0.93 ^c	Cui et al. 2012
<i>U. Pumila</i>	Sandy soil	95	5	Well	High amplitude area	0.9	30	0.96, 0.97 ^c	Cui et al. 2012
<i>U. Pumila</i>	Sandy soil	95	5	Well	High amplitude area	2.0	25	0.90, 0.92 ^c	Cui et al. 2012

[†] With the exceptions of Cui et al. (2011) and Cui et al. (2012) which were conducted under controlled conditions and aimed at both root fresh weight and root biomass estimation, other studies were completed under natural conditions in the field for root biomass estimation

*Speculated values according to the reported soil types, based on the National Cooperative Soil Survey database of the U.S. (<http://websoilsurvey.nrcs.usda.gov>)

^a Values listed before parenthesis are sample size or corresponding correlation coefficient between root biomass and GPR indices from total sampled soil cores; values in parenthesis correspond to correlation coefficient between averaged coarse root biomass and GPR indices in a subplot (or block)

^b The first value corresponds to coefficient between live root biomass and GPR index, and the second value corresponds to the coefficient between combined live and dead root biomass and GPR index

^c The correlation coefficients between GPR index and root fresh weight; other values are the correlation coefficients between GPR index and root biomass

dry wood (4.5) and air (1), the dielectric constant of root (i.e., a combination of dry wood, air, and water) is dominated by its water content (al Hagrey 2007). Furthermore, electrical conductivity of woody material is strongly correlated with water content (Forest Products Laboratory 1999; Straube et al. 2002). Therefore, root water content is an important control of root radar signal.

In previous studies, root biomass was inferred from radar-reflectance related GPR indices, including areas within threshold range, reflector tally (i.e., manual root reflector counts on radargrams), and pixels within the threshold range (Table 1). Because root water content strongly influences root radar reflectance and root biomass (i.e., a measurement of root dry weight) is not dependent on water content, previous GPR-based root biomass estimation is questionable. However, no study has quantitatively evaluated the impact of root water content on root biomass quantification using GPR. Only Hirano et al. (2009) concluded that accurate root biomass could not be estimated using the single frequency of GPR when the water content of roots and soils were unknown.

For these reasons, the objectives of this study are two-fold: 1) to evaluate the impact of root water content on GPR-based root biomass estimation in a sandy area; and 2) to improve the accuracy of root biomass estimation using GPR, especially when studied roots exhibit a broad range of root water content. It is hypothesized that root GPR reflectance is determined by both root biomass and root water content, and the accuracy of GPR-based root biomass estimation declines as the range of root water content extends. To test the hypothesis, results from theoretical forward simulations were integrated into field controlled experiments. The simulations were synthesized following the protocol presented in our companion paper (Guo et al. 2013b), based on which specific GPR radargrams could be simulated corresponding to roots with various combinations of water contents and biomasses.

Materials and methods

Field root water content investigation in sandy soils

In June 2008 and June 2011, field investigations of root water content were conducted at the Maowusu Sandy Land (37°28′~39°22′N, 107°20′~110°30′E) and

the Hunshandak Sandy Land (42°23′~43°56′N, 112°10′~116°52′E) in Inner Mongolia, China. These arid and semi-arid areas in northern China have deep, excessively drained, rapidly permeable, and low organic content sandy soils (Su et al. 2006; Yamanaka et al. 2007), which provide suitable field conditions for conducting GPR root investigations as recommended by Butnor et al. (2001). A total of thirty-six plants belonging to five species (*Artemisia ordosica* Krasch, *Caragana microphylla* Lam, *Caragana korshinskii* Kom, *Salix psammophila* C. Wang et Chang Y. Yang, and *Ulmus pumila* Linnaeus) were collected in the field (Table 2). In addition to the 254 roots used for developing the Root Length-Biomass Model in the companion paper (Guo et al. 2013b), samples from another three *C. microphylla* plants and seven *C. korshinskii* plants were added in this study, resulting in a total of 409 root samples (Table 2).

Roots of *A. ordosica*, *C. korshinskii*, and *S. psammophila* were collected at the Maowusu Sandy Land, where *A. ordosica*, *C. korshinskii* dominated the semi-shifting sand dunes, whereas *S. psammophila* often distributed on the relative flat regions between sand dunes. Roots of *C. microphylla* and *U. pumila* were collected at the Hunshandak Sandy Land, where *U. pumila* formed sparse forests in the center of the sandy land, and *C. microphylla* dominated the transition zone between sandy land and grassland. In each sandy land, five study sites (with at least 30 km between neighboring sites) were chosen for collecting roots, where a soil pit (1 m long and 1.5 m deep) was dug beside each selected plant. Living roots with various diameters were then randomly collected. Once excavated, fresh weights and diameters of roots were measured immediately (Table 2). All samples were then taken back to laboratory and oven dried at 65 °C until constant root weights were reached. Root biomass (i.e., root dry weight) and root water content (i.e., the gravimetric water content of the root defined as the ratio of root water mass to root dry weight) were obtained, providing a reference for the simulated root water content range in our forward simulations.

Soil samples were also taken from five depths (0–15, 15–30, 30–50, 50–70, and 70–90 cm) near each studied plant (except for *U. pumila*) using a Dutch auger (5 cm inner diameter and 1 m length). Soil gravimetric water contents were calculated by soil fresh weights measured in situ and over dried weights determined in laboratory (drying at 105 °C until constant weight was reached) (Table 3).

Table 2 Root samples collected in the sandy soil of northern China, including plant species, number of sampled roots, number of sampled plants, average and range of root diameters, and the frequency distribution as well as water content range in each root diameter class

Species	No. of sampled roots	No. of sampled plants	Average and range of root diameter (cm)	Frequency distribution and water content range (mean \pm S.D.) ^a in each root diameter class (cm)				
				0.2–0.5	0.5–1.0	1.0–2.0	2.0–3.0	>3.0
<i>A. ordosica</i>	42	5	0.87 (0.31–1.93)	19 % (147 \pm 19 %)	45 % (157 \pm 37 %)	36 % (141 \pm 31 %)	0 %	0 %
<i>C. micropophylla</i>	122	8	0.75 (0.21–3.26)	18 % (116 \pm 41 %)	61 % (108 \pm 23 %)	17 % (102 \pm 24 %)	2 % (97 %)	2 % (122 %)
<i>C. korshinskii</i>	156	12	0.83 (0.20–3.84)	22 % (107 \pm 25 %)	49 % (115 \pm 28 %)	25 % (118 \pm 29 %)	2 % (105 %)	1 % (102 %)
<i>S. psammophila</i>	53	6	0.69 (0.21–1.54)	30 % (113 \pm 33 %)	55 % (115 \pm 23 %)	15 % (105 \pm 27 %)	0 %	0 %
<i>U. pumila</i>	36	5	1.92 (0.49–3.90)	3 % (131 %)	14 % (102 \pm 12 %)	42 % (105 \pm 23 %)	25 % (125 \pm 13 %)	17 % (119 \pm 14 %)

^a Gravimetric root water content range; if the number of root sample is less than 5 in any diameter class, only the average water content is listed

Forward simulation

Scenario I: variation of root GPR signals at different root water content levels

The goal of simulation *Scenario I* was to examine the variation of radar signals for roots with same biomass but different water contents. These scenarios were conducted using *GprMax*, which is a Finite-Difference Time-Domain based GPR simulator that generates radar responses based on the input EM properties of reflectors and radar antenna related parameters (Giannopoulos 2005). Because root biomass could not be directly input as an initial parameter in *GprMax*, root biomass levels were represented by various root diameters, based on the strong one-to-one correspondence between root biomass per unit length and root diameter (i.e., the Root Length-Biomass Model presented in Guo et al. 2013b; also see Hirano et al. 2012). Since only roots with diameters larger than 0.5 cm could be clearly detected by GPR even under favorable field conditions (Butnor et al. 2001), three diameter classes of 1, 2, and 5 cm were designed to represent a root biomass gradient. Eight root gravimetric water content levels from 10 to 150 %, with increments of 20 %, were set to establish a root water content gradient.

Simulations were computed under three high antenna center frequencies of 0.5, 0.9, and 2.0 GHz, as they were commonly selected for root investigations (Table 1). A total of 72 root GPR radargrams (i.e., 3 root biomass classes \times 8 root water content levels \times 3 simulated antenna center frequencies) were simulated based on the protocol presented in Guo et al. (2013b).

For each simulation, 54 synthetic traces were generated to represent GPR signals from a root sample at 30 cm depth surrounded by sandy soil with a volumetric water content of 10.5 % (based on measurements at the field experiment site). Figure 1a illustrates the geometric configuration of each simulation. A Ricker pulse (the first derivative of a Gaussian pulse) was selected as the source wavelet. Taking into consideration both numerical stability and model reliability, the spatial discretization was set to 1.5 mm. The time window of each trace was set to 20 ns. The third order Higdon absorbing boundary condition was selected to simulate the open boundary condition. The rationales for the simulation parameters are provided in Guo et al. (2013b) and Giannopoulos (2005).

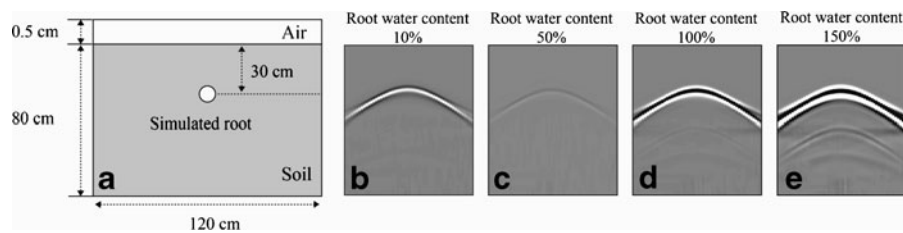


Fig. 1 a) Illustration of geometric domain used in forward simulation; b), c), d), and e) are synthetic radargrams for roots with the same diameter (2 cm) and buried depth (30 cm) but different water contents (10 to 150 %), simulated with 0.9 GHz

Scenario II: root biomass estimation using GPR at different root water content ranges

In accordance with the results of field investigations (Fig. 2), seven gravimetric water content levels from 90 to 150 %, with increments of 10 %, were set to represent common water conditions of roots in the studied sandy areas. Twenty root diameter classes (i.e., 0.4 to 4.2 cm, with increments of 0.2 cm) were set to represent 20 root biomass levels. A total of 420 root GPR radargrams (20 root biomass levels \times 7 root water content grades \times 3 antenna center frequencies) were simulated. The general settings were kept the same as in simulation *Scenario I*.

Three gravimetric root water content spans (110~130 %, 100~140 %, and 90~150 %) were selected to stand for roots with narrow (<20 %), medium (20~40 %), and wide (>40 %) water content ranges, respectively. Taking into consideration the normal distribution pattern of root water contents in the study areas (Fig. 2), 45 simulated root radargrams were resampled from simulation *Scenario II* for each investigated root water content range following the strategy shown in Table 4 to ensure that the simulated root samples would have a similar water content distribution to those collected in the field.

antenna center frequency and volumetric water content of sandy soil background at 10.5 %. Reflected parabola on each radargram is root GPR signal

Field controlled experiments

The field controlled experiments were conducted in the southern part of the Hunshandak Sandy Land (42°26'N, 116°11'E). Roots of *U. pumila* were grouped into six classes (with average diameters of 0.5, 1, 1.5, 2, 2.5, and 3.5 cm) and then were inserted into ground as target reflectors at known depths. A field portable GPR system Zond-12e (Georadar Systems, Inc., Latvia) with three shielded antenna pairs with center frequencies of 0.5, 0.9, and 2.0 GHz was used for data collection. After field experiments, all roots were taken back to laboratory and oven dried at 65 °C until constant root dry weight reached to measure root biomass and water content (Table 5). Detailed description of field experiment can be found in our previous study, Cui et al. (2012).

Post processing of GPR data and extraction of GPR indices

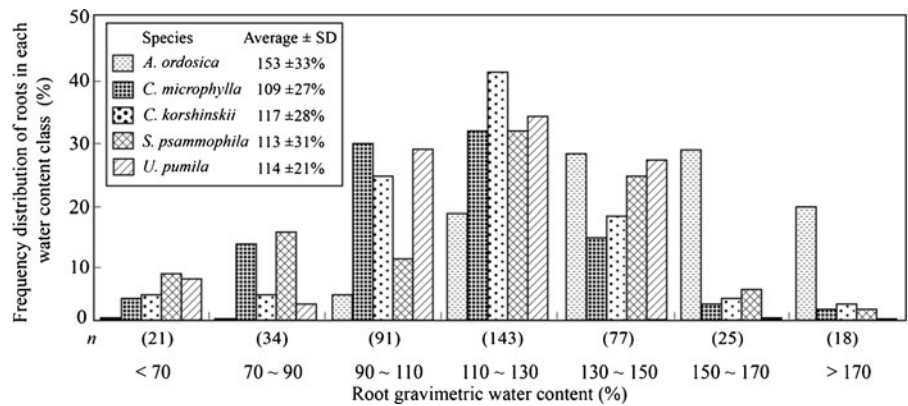
The post-processing procedures performed on raw simulated radargrams included background removal, Kirchhoff migration, and Hilbert transform. A referential background radargram was simulated corresponding to the computing domain with the same geometric configuration shown in Fig. 1a but

Table 3 Soil water content at different depths in the sampling plots of four studied species in the sandy land of northern China

Species ^a	No. of soil cores sampled	Gravimetric soil water content (mean \pm S.D.) at each depth interval (cm)				
		0–15	15–30	30–50	50–70	70–90
<i>A. ordosica</i>	8	2.4 \pm 0.4 %	3.9 \pm 1.5 %	5.6 \pm 1.8 %	7.6 \pm 1.3 %	7.0 \pm 2.0 %
<i>C. microphylla</i>	12	1.5 \pm 0.5 %	2.4 \pm 0.6 %	2.3 \pm 0.5 %	2.1 \pm 0.5 %	1.5 \pm 0.6 %
<i>C. korshinskii</i>	17	1.3 \pm 0.7 %	2.7 \pm 1.2 %	2.6 \pm 0.5 %	3.3 \pm 0.9 %	3.8 \pm 1.2 %
<i>S. psammophila</i>	10	7.1 \pm 2.2 %	5.7 \pm 1.8 %	14.5 \pm 2.6 %	24.6 \pm 0.6 %	25.8 \pm 0.9 %

^a Soil cores were not sampled in the *U. pumila* plots

Fig. 2 Frequency of roots in each root water content class for five species sampled in the sandy soil of northern China. Gravimetric root water content (average ± S.D.) is indicated for each species. *n* is total root number of the five species in each water content class



excluding root reflector. Background removal was then achieved using a program compiled in MATLAB (The MathWorks, Inc., USA), which deleted the background radargram from the simulated root radargram. Kirchhoff migration was performed on each root radargram to trace the hyperbolic root GPR signal to its source (Daniels 2004). Radar wave velocity, an input parameter of Kirchhoff migration, was estimated by hyperbola fitting (Barton and Montagu 2004). Finally, the Hilbert transform was performed to reconstruct the phase of the signal from its amplitude (Oppenheim and Schaffer 1975; Stover et al. 2007). Kirchhoff migration (including wave velocity estimation) and the Hilbert transform were processed with Reflex-Win 5.0 (Sandmeier Scientific Software, Karlsruhe, Germany).

The sequence of raw field GPR data processing included break correction, background removal, amplitude compensation, Kirchhoff migration, and Hilbert transform. The first step was to detect the first break time of each trace and correct the drift of first breaks along all the traces. Then, a high-pass filter and a low-pass filter were successively applied to the field radargram to remove horizontal

bands and high-frequency noise, respectively. The impact of radar energy attenuation was calibrated by amplitude compensation (Cui et al. 2012). Generally, GPR wave amplitude decays exponentially with propagation time (al Hagrey 2007). The measured amplitude, $A(f,t)$, and the compensated amplitude without energy attenuation, A_0 , have the following relationship (Turner and Siggins 1994; Neto and de Medeiros 2006):

$$A(f, t) = A_0 \exp(-\alpha^* t), \tag{2}$$

where f is the antenna center frequency, t is the travel time of radar energy, and α^* is a frequency dependent attenuation factor that determines the extent of radar energy attenuation within a particular medium. The value of α^* of the experimental soil was estimated based on a smoothed Hilbert transform of a representative data volume for each investigated antenna center frequency (Truss et al. 2007). Field root radargrams were calibrated using the calculated attenuation factor. Finally, Kirchhoff migration and Hilbert transform were performed on

Table 4 Number of simulated root radargrams resampled from simulation Scenario II for assessing root biomass estimation accuracy using GPR at each root water content range investigated

Gravimetric root water content range investigated (%)	Total number of resampled root radargrams	Number of root radargrams resampled from simulation Scenario II at each simulated gravimetric root water content level						
		90 %	100 %	110 %	120 %	130 %	140 %	150 %
110~130	45	0	0	19	16	10	0	0
100~140	45	0	6	14	12	7	6	0
90~150	45	3	5	12	10	6	5	4

Table 5 Selected GPR indices (*Parea*, *Pixels*, and *dT*) extracted from the field collected GPR data under three antenna frequencies (0.5, 0.9, and 2.0 GHz). The actual root diameter, fresh weight, water content, and buried depth for each root investigated are shown

Root no.	Diameter (mm)	Fresh weight (g) ^a	Biomass (g) ^a	Gravimetric root water content (%)	Buried depth (cm)	<i>Parea</i> (normalized amplitude×ns)			<i>Pixels</i> (no.)			<i>dT</i> (ns)		
						0.5 GHz	0.9 GHz	2.0 GHz	0.5 GHz	0.9 GHz	2.0 GHz	0.5 GHz	0.9 GHz	2.0 GHz
1a	37.0	602	246	145	10	1.69	1.16	0.53	6099	5797	5292	4.49	3.18	2.11
1b	37.6	656	317	107	20	1.40	0.70	0.33	4988	4367	3753	4.15	3.22	1.99
1c	33.7	547	231	136	30	1.56	1.01	0.48	5338	5135	4717	4.23	2.83	1.97
1d	39.0	682	306	123	40	1.54	0.97	0.42	5563	5023	4478	4.45	3.10	2.10
1e	37.3	640	288	122	60	1.42	0.83	0.39	5098	4583	4054	4.06	2.72	2.06
1f	37.1	634	266	138	80	1.64	1.20	–	6127	5946	–	4.22	2.86	–
2a	26.2	281	136	107	10	0.51	0.28	0.17	2011	1960	1823	3.58	2.46	1.80
2b	25.6	349	149	134	20	1.03	0.67	0.33	3769	3596	3313	3.74	2.42	1.77
2c	26.6	359	150	139	30	1.05	0.71	0.36	3759	3695	3121	3.82	2.67	1.84
2d	24.9	291	137	112	40	0.52	0.34	0.19	2091	1782	1743	3.51	2.34	1.75
2e	24.2	264	114	131	60	0.85	0.53	0.28	2968	2960	2505	3.37	2.29	1.62
2f	25.7	302	139	117	80	0.80	0.39	–	2240	2105	–	3.59	2.38	–
3a	19.5	156	70	122	10	0.62	0.17	0.19	1821	2282	1988	3.25	2.22	1.58
3b	21.3	201	94	113	20	0.39	0.21	0.16	1423	1425	1495	3.15	2.24	1.59
3c	22.3	210	91	131	30	0.50	0.45	0.24	2322	2272	2701	3.27	2.33	1.62
3d	22.0	212	87	144	40	0.77	0.56	0.27	2636	2616	2246	3.58	2.38	1.66
3e	19.4	162	77	112	60	0.44	0.35	0.10	1033	1023	1320	3.01	2.16	1.66
3f	19.5	176	76	130	80	0.62	0.40	–	2096	2440	–	3.35	2.09	–
4a	13.5	88	42	112	10	0.37	0.11	0.09	615	848	874	3.05	1.98	1.52
4b	17.4	118	71	66	20	0.29	0.08	0.07	711	633	623	3.17	2.06	1.50
4c	15.3	121	56	115	30	0.39	0.16	0.13	1202	922	609	3.26	2.14	1.49
4d	17.1	139	69	101	40	0.39	0.20	0.12	943	1140	958	3.22	2.15	1.46
4e	15.1	116	56	108	60	0.49	0.16	0.11	925	987	915	2.97	2.09	1.56
4f	14.0	93	42	121	80	–	0.14	–	–	1189	–	–	2.01	–
5a	11.1	62	32	97	10	–	0.08	0.05	–	546	407	–	1.87	1.45
5b	11.6	67	33	103	20	–	0.09	0.06	–	947	518	–	1.90	1.56
5c	10.4	45	21	118	30	–	0.13	0.09	–	429	235	–	1.69	1.51

Table 5 (continued)

Root no.	Diameter (mm)	Fresh weight (g) ^a	Biomass (g) ^a	Gravimetric root water content (%)	Buried depth (cm)	<i>Parea</i> (normalized amplitude×ns)			<i>Pixels</i> (no.)			<i>dT</i> (ms)		
						0.5 GHz	0.9 GHz	2.0 GHz	0.5 GHz	0.9 GHz	2.0 GHz	0.5 GHz	0.9 GHz	2.0 GHz
5d	11.7	57	25	133	40	–	0.16	0.13	–	1284	970	–	1.95	1.53
5e	11.5	58	32	83	60	–	0.07	–	–	684	–	–	1.77	–
5f	12.6	56	37	52	80	–	–	–	–	–	–	–	–	–

^a Fresh weight and biomass of each root, not per unit length

–Root was not detected in the field

the field collected radargrams. All these processes were completed using Reflex-Win 5.0.

In previous studies (e.g., Butnor et al. 2001, 2003; Stover et al. 2007; Samuelson et al. 2008), the number of pixels within the threshold range extracted on the gray scaled radar images (converted from root radargrams after Hilbert transform) was most commonly used for root biomass estimation (Table 1). This GPR index measures the intensity (a measurement of relative signal strength) of each pixel on the radar image and counts the number of pixels with intensities above a threshold value (Cox et al. 2005). Thus, the number of pixels within the threshold range is radar signal-strength related. In other words, it was the root radar reflectance that was used for root biomass estimation. In order to achieve a better characterization of root radar reflectance, both pixels within the threshold range and the high amplitude area (a direct indicator of radar reflectance, which is also used for sizing roots) were analyzed in this study.

To increase the comparability of our results with other studies, before GPR indices extraction, reflection amplitudes of the simulated data and the field collected data were first divided by the simulated maximum reflected amplitude and the detected maximum reflected amplitude after energy attenuation compensation, respectively, to linearly normalize the amplitude data. After amplitude normalization, high amplitude areas of the maximum and minimum reflected waves were extracted from the trace passing through the center of each root after migration (Fig. 3) and the sum of their absolute values was defined as *Parea*. Then, pixels within the threshold range (i.e., *Pixels*) were measured on 8-bit gray scale root radar images converted from radargrams after Hilbert transform. Radar image conversion was accomplished using Reflex-Win 5.0. *Parea* and *Pixels* were extracted using a code compiled in MATLAB and Sigma Scan Pro 5.0 (Systat Software Inc., USA), respectively. In addition to the radar-reflectance related GPR indices, the time interval index (i.e., *dT*, the sum of the time interval between zero crossings of the maximum and the minimum reflected waves; see illustration in Fig. 3), which is a GPR index originally designed for root diameter estimation (e.g., Barton and Montagu 2004; Cui et al. 2011), was extracted from the trace passing through the center of each root using the code developed in MATLAB after the process of Kirchhoff migration. For our field data, average indices extracted for each root on six transects were used in the following statistical analysis.

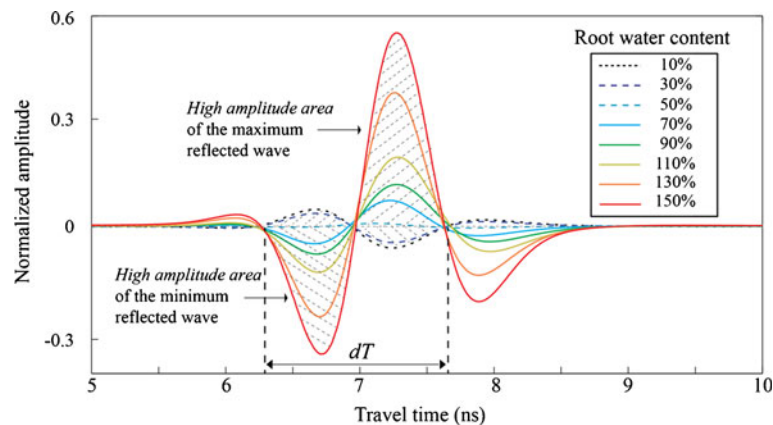


Fig. 3 Waveform variation of radar reflections for roots with the same diameter (2 cm, indicating the same root biomass) but different root water contents (10 to 150 %, with increments of 20 %), simulated with 0.9 GHz antenna center frequency and water content of sandy soil background at 10.5 %. Vertical

Linear and quadratic regression models of root biomass on GPR indices and root fresh weight on GPR indices were developed using SPSS for Windows 13.0 (SPSS Inc., USA). Data used for regression model development and correlation analysis all passed the normal distribution test. For the simulated data, root fresh weight was calculated from root biomass and root water content based on the Root Length-Biomass Model and the Root Composition Model, described in Guo et al. (2013b). The coefficient of determination (R^2) and root mean square error (RMSE) were used for evaluating the correlation between GPR indices and root biometric parameters (i.e., root biomass and fresh weight) and the estimation accuracy of each model, respectively.

Results

Root water content in sandy soils of northern China

In general, all studied species exhibited a broad variability in root water content (Fig. 2). The smallest root gravimetric water content variation was over 125 %, seen in *U. pumila*, while the largest variation reached 204 %, seen in *C. korshinskii*. Regardless of root diameter class, most studied species revealed similar average root gravimetric water contents of ~115 % except for *A. ordosica* (which had an average water content of 153 %) (Fig. 2). Figure 2 also demonstrates a normal

dashed lines define the time interval between zero crossings of the maximum and minimum reflected waves (i.e., dT). The oblique dashed lines define the high amplitude area of the maximum and minimum reflected waves

distribution pattern of root water content, with majority varying from 90 % to 150 %.

Most root samples (over 45 %) of shrub species (i.e., *A. ordosica*, *C. microphylla*, *C. korshinskii*, and *S. psammophila*) were between 0.5 and 1.0 cm in diameter, with the average root diameters ranging from 0.69 to 0.87 cm. In comparison, for the tree species (i.e., *U. pumila*), 42 % of root samples were between 1.0 and 2.0 cm in diameter, with an average diameter of 1.92 cm (Table 2). Correlation of root diameter to root water content was poor ($P > 0.5$), as all studied species showed broad water content ranges in any diameter class (Table 2). We were unable to correlate root water contents of each species to in situ soil water contents (Fig. 2 and Table 3). These results of field root water content investigations suggested that the wide variability in root water content is common for roots in the sandy lands of northern China, regardless of species, root diameters, and soil water contents.

Impact of root water content on root radar signal

Based on simulation *Scenario I*, waveforms of traces passing through the center of simulated roots were extracted after background removal. In any root water content level, the series of waveforms shared a similar oscillation pattern that the polarity of radar pulses changed when radar wave reached the root-soil interface (Fig. 3). However, the normalized amplitudes and high amplitude areas of the waveforms were divergent among

different root water contents: roots with a gravimetric water content of 50 % showed the minimum magnitude of radar signal; when root water content was below 50 %, radar signal amplitudes negatively correlated with root water content; whereas radar signal amplitudes magnified with increased root water content when root water content was above 50 % (Fig. 3). Phase positions of waveforms were opposite for roots with water content below and above 50 %. These results of waveform variations closely followed the trend observed for root signals (i.e., hyperbolic reflections) on simulated radargrams (Fig. 1b, c, d, e). Different from amplitude and high amplitude area, time intervals between the zero crossings of both the maximum and minimum reflected waves vary slightly along root water content gradient (Fig. 3).

For all synthesized radargrams in simulation *Scenario I*, three GPR indices (*Parea*, *Pixels*, and *dT*) were extracted. To avoid interference from GPR detection resolution, data simulated for roots with the diameter of 1 cm and with 0.5 GHz antenna frequency were excluded in Fig. 4. At all root biomass levels and simulation frequencies, when root water content was below 50 %, reflectance related GPR indices (*Parea* and *Pixels*) decreased as root water content increased and reached the minimum when root water content was at 50 %; however, when root water content was above 50 %, *Parea* and *Pixels* positively correlated to root water content (Fig. 4a, b).

The sensitivity of the time interval index (*dT*) to root water content differed among various root biomass levels and simulation antenna frequencies (Fig. 4c): for larger root (5 cm in diameter), a clear increase of *dT* with the increase of water content was found at all simulation frequencies when root water content was above 50 %; for root with a simulated diameter of 2 cm, the increase of *dT* along the root water content gradient was observed at higher simulation frequencies (0.9 and 2.0 GHz) when root water content was above 70 %; and for the smaller root (1 cm in diameter), *dT* increased slightly with increased root water content only at the highest simulation frequency (2.0 GHz) and when root water content was over 110 %.

In the field controlled experiments, 0.5 GHz GPR system achieved a better penetrating depth but a coarser detection resolution such that all roots with a diameter class of 1 cm were unable to be resolved by antenna (Table 5). 2 GHz GPR system had a finer detection resolution but a shallower observation depth, and all the roots buried at

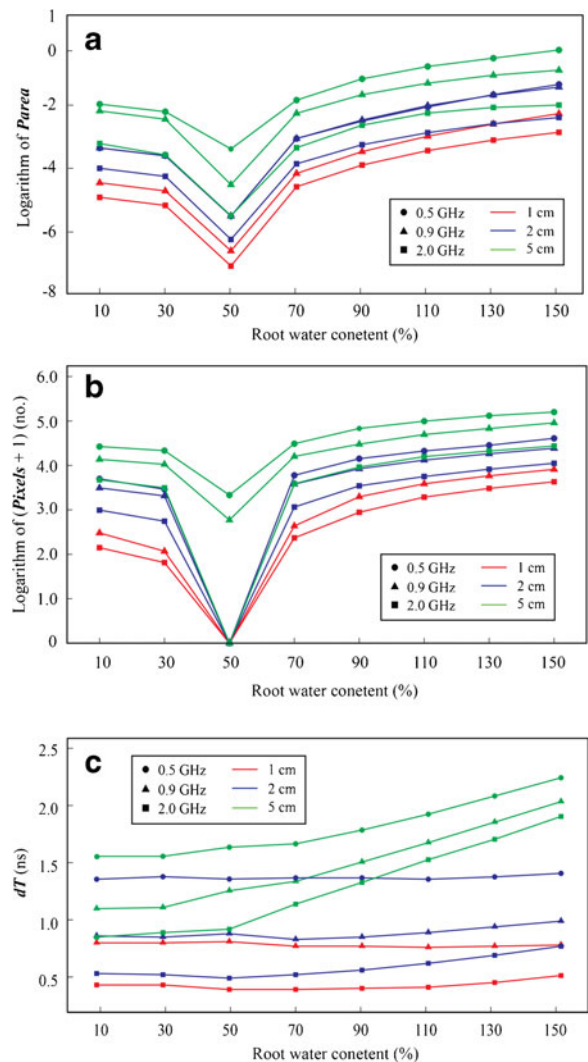
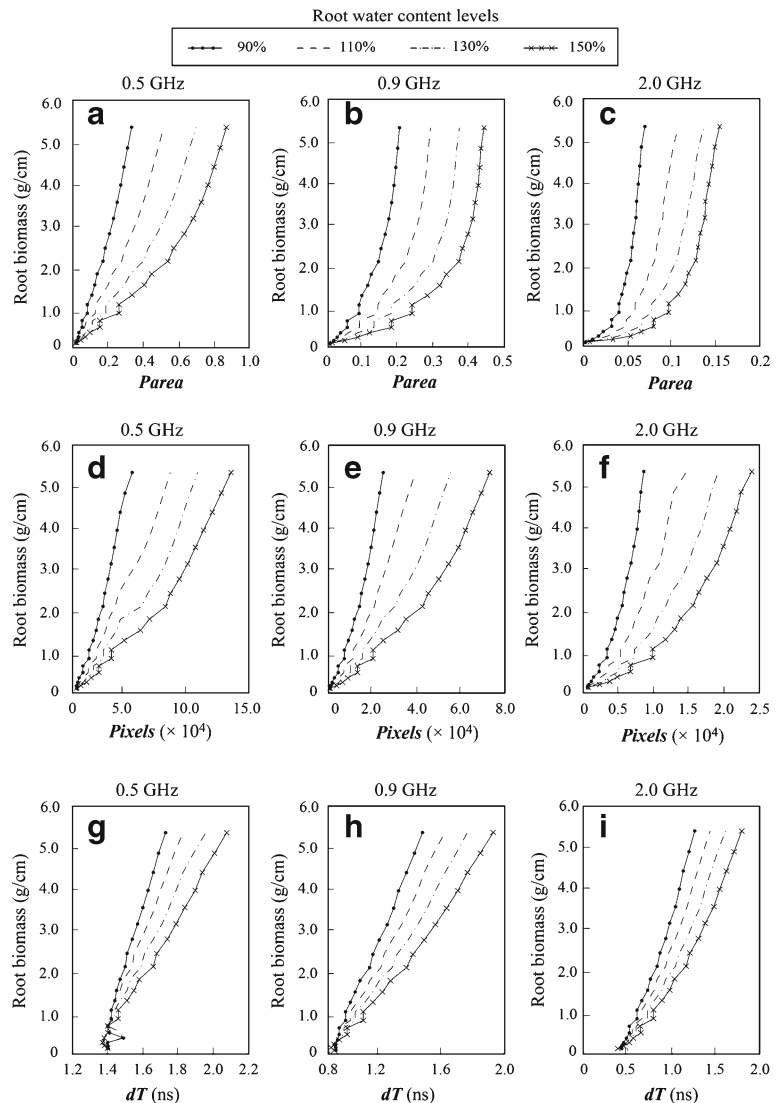


Fig. 4 a) High amplitude areas (*Parea*), b) pixels within the threshold range (*Pixels*), and c) time interval (*dT*) extracted from reflected waveforms and radar images of roots, with simulations being computed along root water content gradient (10 to 150 %, with increments of 20 %), at different root diameter levels (1, 2, and 5 cm, indicating three root biomass levels), and under three antenna center frequencies (i.e., 0.5, 0.9, and 2.0 GHz). Data simulated for roots at 1 cm diameter and with 0.5 GHz frequency are excluded to avoid the bias from GPR resolution

80 cm could not be detected by antenna (Table 5). The 0.9 GHz GPR system achieved the best detection outcome with only one small root buried in deep soil being undetectable. All the undetected roots were excluded from further analysis (Table 5).

Table 5 lists the values of *Parea*, *Pixels*, and *dT* extracted from the field collected radargrams. At each

Fig. 5 Regression relationships between root biomass and GPR indices (**a**, **b**, and **c**: *Parea*; **d**, **e**, and **f**: *Pixels*; and **g**, **h**, and **i**: *dT*) at different root water content levels (90 to 150 %, with increments of 20 %) and different antenna center frequencies (0.5, 0.9, and 2.0 GHz)



antenna center frequency, roots from larger diameter classes (indicating higher root biomass) resulted in higher GPR indices. However, within each diameter class (indicating similar root biomass), root water content had a significant effect on reflectance related GPR indices (*Parea* and *Pixels*). For example, within the five root pairs (i.e., 1b and 1c, 2a and 2e, 3b and 3d, 4a and 4b, and 5b and 5d), roots with a smaller biomass but higher root water content (roots 1c, 2e, 3d, 4a, and 5d) resulted in higher *Parea* and *Pixels* than roots with a larger biomass but lower root water content (roots 1b, 2a, 3b, 4b, and 5b), regardless of antenna center frequency (Table 5). Results from forward simulation and field experiment both supported our hypothesis that GPR

indices depend on both root biomass and root water content.

Impact of root water content on root biomass estimation using GPR

Root biomass was correlated to GPR indices at four root water content levels (Fig. 5). Figure 5 clearly shows that the relationships between GPR indices and root biomass diverged at different root water content levels. This suggests that any GPR index value could result from various combinations of root biomass and root water content. Consequently, larger residual errors (or lower predictive

accuracy) of the fitted regression model between root biomass and GPR indices would be expected with greater variability in root water content.

Among three selected indices, the variation of correlation between GPR indices and root biomass at different root water content levels was the least for *dT* (Fig. 5), which implies a higher accuracy of root biomass estimation using *dT*. For *Parea* and *Pixels*, their correlation with root biomass became nonlinear with increased root water content and antenna center frequency (Fig. 5). However, all previous studies that used GPR to estimate root biomass restricted their models to linear regression.

According to the resampling strategy listed in Table 4, linear regression models were developed between root biomass and GPR indices at three root water content ranges (110~130 %, 100~140 %, and 90~150 %). For all GPR indices at each simulated frequency, the coefficient of determination (R^2) decreased when root water content range increased (Table 6). Thus, the prediction accuracy of such regression model was negatively correlated with the range of root water content. Among different GPR indices, time interval index (*dT*) achieved a better predictive accuracy (indicated by higher R^2 values) than *Parea* and *Pixels*. Moreover, for *Parea* and *Pixels*, R^2 decreased with the increase of simulated

frequency, whereas R^2 minimally varies with simulated frequency increasing for *dT* (Table 6).

Regression analysis revealed a higher R^2 between GPR indices and root fresh weight for all studied root water content ranges (Table 6). As root water content range extends, improvement of R^2 resulted from using root fresh weight instead of root biomass was more significant (Table 6), proving the impact of water content on root biomass quantification. Among the selected GPR indices, correlating fresh weight to root biomass led to the least R^2 change for *dT* (Table 6), which indicated a relatively limited sensitivity of *dT* to root water content.

Limited by sample numbers, root fresh weight from our field data were correlated to root biomass without differentiating root water content ranges (Table 6). Consistent with results from the theoretical forward simulation, higher R^2 values were obtained from regression models between GPR indices and root fresh weight for any antenna center frequency. As shown in Tables 6, the linear correlation between *Parea/Pixels* and root biomass/fresh weight decreases with the increase in antenna center frequency; however, the correlation between *dT* and root biometric parameters strengthens with the increase in antenna center frequency.

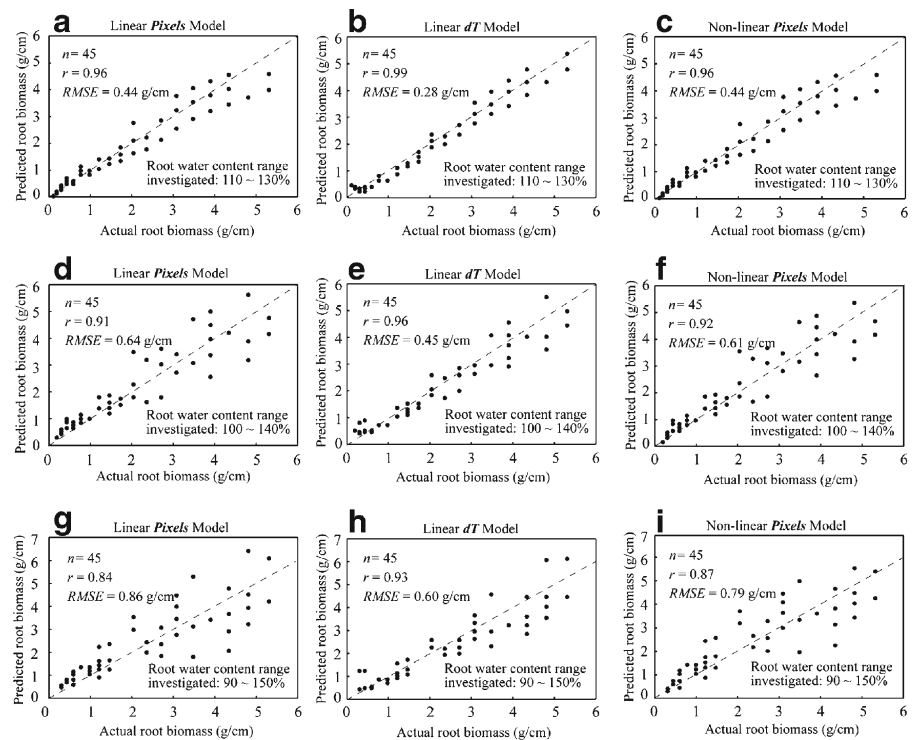
Table 6 The coefficient of determination (R^2) of fitted regression models between selected GPR indices (high amplitude area, *Parea*; pixels within threshold range, *Pixels*; and time interval, *dT*) and root biometric parameters (root biomass and

fresh weight) obtained from both simulated and field collected GPR data under three antenna center frequencies. All R^2 passed the 0.001 significance test

Antenna center frequency (GHz)	GPR index	Simulation data						Field collected data	
		110 %~130% ^a		100 %~140% ^a		90 %~150% ^a		Biomass	Fresh weight
		Biomass	Fresh weight	Biomass	Fresh weight	Biomass	Fresh weight		
0.5	<i>Parea</i>	0.92	0.94	0.90	0.93	0.82	0.89	0.84	0.90
	<i>Pixels</i>	0.94	0.96	0.91	0.95	0.84	0.91	0.86	0.92
	<i>dT</i>	0.96	0.97	0.94	0.97	0.91	0.96	0.87	0.91
0.9	<i>Parea</i>	0.81	0.82	0.73	0.78	0.61	0.70	0.78	0.85
	<i>Pixels</i>	0.92	0.94	0.82	0.88	0.69	0.80	0.83	0.89
	<i>dT</i>	0.98	0.99	0.95	0.98	0.91	0.97	0.91	0.92
2.0	<i>Parea</i>	0.75	0.77	0.71	0.75	0.67	0.74	0.73	0.81
	<i>Pixels</i>	0.88	0.90	0.83	0.88	0.76	0.84	0.81	0.87
	<i>dT</i>	0.97	0.98	0.95	0.98	0.93	0.97	0.91	0.93

^a Gravimetric root water content range investigated

Fig. 6 Accuracy comparison among three root biomass estimation methods at three different root gravimetric water content ranges (a, b, and c: 110 to 130 %; d, e, and f: 100 to 140 %; and g, h, and i: 90 to 150 %) with the simulation antenna frequency of 0.5 GHz: 1) Linear *Pixels* Model (a, d, and g); 2) Linear *dT* Model (b, e, and h); and 3) Non-Linear *Pixels* Model (c, f, and i). On each graph, the sample number (n), correlation coefficient (r), prediction root mean square error ($RMSE$), and the 1:1 line are shown. Actual root biomass is calculated from root diameter and root water content



The above results from both theoretical forward simulation and field controlled experiment confirm the significant effect of root water content on root GPR indices and the estimation of root biomass using GPR.

Two new approaches of root biomass estimation using GPR

Based on the data from simulation *Scenario II*, Fig. 6 compares the accuracies of root biomass estimation using three types of regression model, including 1) the linear regression model between *Pixels* and root biomass (Linear *Pixels* Model), 2) the linear regression model between *dT* and root biomass (Linear *dT* Model), and 3) the quadratic regression model between *Pixels* and root biomass (Non-linear *Pixels* Model). The Linear *Pixels* Model, broadly applied in previous studies to GPR-based root biomass estimation was set as the reference for evaluating the performance of our proposed new approaches. Given that the accuracy of the Linear *Pixels* Model is higher at lower antenna center frequency, 45 root radargrams simulated with 0.5 GHz were selected for model development following the resample strategy, shown in Table 4. Another 45 root radargrams simulated with

0.5 GHz were resampled following the same strategy for model validation. The predicted root biomass from the three estimation models were plotted against the actual root biomass at various root water content ranges (calculated from the root diameter and root water content) (Fig. 6). The Linear *dT* Model achieved the best estimation accuracy, regardless of root water content range investigated (Fig. 6b, e, h). Under narrow root water content range (from 110 % to 130 %), the difference in estimation accuracy is not noticeable between the Linear *Pixels* Model and the Non-linear *Pixels* Model (Fig. 6a, c). However, under medium and wide root water content ranges (from 100 % to 140 %, and from 90 % to 150 %, respectively), the Non-linear *Pixels* Model yielded more accurate estimates than the Linear *Pixels* Model (Fig. 6d, f, g, i).

Limited by sample number of the field collected data, leave-one-out cross validation method (*LOOCV*) was applied to evaluate the accuracy of the three methods. Regardless of antenna center frequency, the Linear *dT* Model and the Non-linear *Pixels* Model achieved a higher estimation accuracy than the Linear *Pixels* Model (Table 7). Simulated and field collected data together suggest that the new methods (the Linear *dT* Model and the Non-linear *Pixels* Model) out-

Table 7 Root biomass estimation accuracy using three models for the field collected GPR data, listing the correlation coefficients (r) between predicted and measured root biomasses and the average root mean square error ($RMSE$) of leave-one-out cross validation

Antenna center frequency (GHz)	Estimation model	r	$RMSE$ (g)
0.5	Linear <i>Pixels</i> Model	0.895	35.97
	Linear <i>dT</i> Model	0.906	33.46
	Non-linear <i>Pixels</i> Model	0.900	34.53
0.9	Linear <i>Pixels</i> Model	0.879	40.50
	Linear <i>dT</i> Model	0.926	31.05
	Non-linear <i>Pixels</i> Model	0.885	38.85
2.0	Linear <i>Pixels</i> Model	0.868	43.32
	Linear <i>dT</i> Model	0.923	30.36
	Non-linear <i>Pixels</i> Model	0.874	41.18

performed the past GPR-based root estimation approach (the Linear *Pixels* Model).

Discussion

The dual dependence of GPR-based root detection and quantification on root size and root water content

The dependence of root detection by GPR on root size (both biomass and diameter) has been recognized (Hirano et al. 2009; Hirano et al. 2012). However, studies concerning the influence of root water content on GPR root detection are limited. Under experimental conditions, Dannoura et al. (2008) and Hirano et al. (2009) reported that both small roots (<1 cm in diameter) and dry roots (water content of roots being lower than that of surrounding soils) were not detected by 0.9 GHz GPR. Similarly, forward simulations in this study suggest that water content gradient between a root and the surrounding soil determines the magnitude of root GPR signals (Figs. 1 and 3), which will influence the detection frequency of a root by GPR.

Most recently, Hirano et al. (2012) correlated the detection frequency of roots on radargram to root size under natural conditions in sandy soils. However, they also found that the detection of roots of similar-sizes was inconsistent (Hirano et al. 2012). In addition to the differences in site-specific soil condition and root depth, this might be caused by the root water content variation among roots with similar size. Our field investigations of 409 roots collected from five common species (four shrub species and one tree species belonging to five families with diameters of sampled roots ranging from 0.2 to 3.9 cm) in sandy lands of northern China demonstrates a broad variation range in root water content

in any root diameter class (Fig. 2, and Table 2). Therefore, roots in sandy soils probably always have a broad range of water content, suggesting that the impact of root water content on GPR-based root study should be taken into account seriously.

The impact of root water content on GPR-based root quantification has not been well recognized (Guo et al. 2013a). To our knowledge, no other study has taken root water content into account when predicting root biomass using GPR. Among previous studies, only Hirano et al. (2009) reported the influence of root water content on the magnitude of signal-strength related GPR indices (including the amplitude of reflected wave and high amplitude area), and indicated that smaller roots with higher water content could generate higher GPR indices than those from larger roots but with lower water content (see Table 1 in Hirano et al. 2009). This study is the first attempt to quantitatively examine the impact of root water content on root GPR indices and the accuracy of root biomass estimation from GPR indices. Forward simulations of roots along a broad water content gradient (10~150 %) show that the signal-strength related GPR indices (*Parea* and *Pixels*) change greatly at different root water content levels even though the root size is the same (Fig. 4). Regression analysis clearly reveals that the relationships between root biomass and GPR indices diverge at different root water content levels, thus proving the double dependence of GPR indices on both root size and root water content (Fig. 5).

Forward simulation data reveal a decreasing trend in the coefficient of determination (R^2) of fitted regression models that link GPR indices and root biomass, as the water content range of studied roots expands (Table 6). Moreover, both field collected and simulated data indicate a stronger correlation between GPR

indices and root fresh weight (which contains both root biomass and root water content) than that between GPR indices and root biomass (Table 6). These results indicate the potential error of root biomass estimation using signal-strength related GPR indices without considering root water content variation.

Estimation accuracy analysis based on simulated data demonstrates that the prediction error of root biomass estimation using *Pixels* doubles from 0.44 g/cm to 0.86 g/cm, when the water content range of studied roots expands from 110–130 % to 90–150 % (Fig. 6a, c). The decrease of estimation accuracy could be explained by the greater influence of root water content on *Pixels* at wider root water content range (Fig. 5d, e, f). This indicates that the past method for root biomass estimation is most appropriate for roots with narrow water content ranges (e.g., variation <20 %).

Evidences from field experiment and forward simulation in this study together suggest that root water content is not only influential for root detection by GPR but also exerts significant impact on GPR-based root biomass estimation. Considering the double dependence of root detection and quantification by GPR on root size and root water content, prior tests on root water content range as well as the detection frequency of roots in different size classes and water content classes are necessary for specific species and sites. In this way, a compensation coefficient for each diameter×water content class can be estimated and thus can increase the estimation accuracy (Hirano et al. 2012).

Improvements in root biomass estimation using GPR

Because of its independence of root depth and radar signal strength, time interval index was originally developed for root diameter quantification (Barton and Montagu 2004). Recently, Cui et al. (2011) successfully correlated time interval index to root fresh weight. We tested the feasibility of using time interval index (dT) for root biomass estimation. Results from forward simulations indicate that dT is not as sensitive to root water content variation as signal-strength related GPR indices are (Figs. 3 and 4), and the relationships between root biomass and dT at different root water content levels are more convergent than those between root biomass and signal-strength related GPR indices (Fig. 5). All these observations suggest a relatively limited impact

of root water content on dT . Both field and simulated data reveals a higher accuracy of root biomass estimation using dT than *Pixels* (Table 6). Under field conditions, the Linear dT Model can decrease root biomass estimation error (*RMSE*) by 4 % to 30 %, when compared to the Linear *Pixels* Model (Table 7). Moreover, simulation data show that the wider the investigated root water content range is, the better the Linear dT Model performs as compared to the Linear *Pixels* Model (Fig. 6).

However, using time interval index for root quantification has not been tested under natural conditions. Good extraction of time interval requires roots being traversed by GPR antenna at 90°, having a level orientation and with no other nearby roots (Barton and Montagu 2004). These limitations prohibit the use of the time interval index under natural conditions (under which roots grow in all directions with varying angles, and often in clumps, and with heterogeneous interactions with soils) (Barton and Montagu 2004). Therefore, this GPR index might be more appropriate for time-lapsed study on lateral roots (with known branching directions).

In comparison to the time interval index, *Pixels* could be suitable for root biomass estimation for roots of any size, angle, and orientation. Based on the finding that *Pixels* nonlinearly correlate to root biomass at high frequency and high root water content (Fig. 5), we tested the accuracy of root biomass estimation using quadratic models of root biomass and *Pixels*. Results from both field and simulated data indicate that the Non-linear *Pixels* model achieves more accurate estimations, especially for roots with wider water content range (>40 %) (Table 7 and Fig. 6).

The form of regression model that links root size into *Pixels* lacks clear physical interpretation. The nonlinear model suggested here is based on the nonlinear correlation between GPR indices and root biomass. Similarly, Hirano et al. (2012) found that root diameter nonlinearly correlated to *Pixels*. For our data, it was the quadratic model that achieved the highest determination coefficient in the regression. Data collected under other conditions may possibly lead to other non-linear regression functions. Therefore, specific nonlinear model should be selected based on specific site and species investigation.

The two optimized methods of root biomass estimation by GPR were developed based on forward simulation and controlled experiments. Our results reveal a better performance of the presented methods in predicting root biomass per unit length (g/cm). However, the accuracy of estimating root biomass per area (g/cm²) using such improved methods should be tested under natural field conditions in future. The complex root branching patterns and the variation in lengths of roots harvested in each soil core would decrease the accuracy of root biomass per area (g/cm²) estimation in the field with the proposed methods.

Other possible improvements in root biomass estimation using GPR

This study indicates that none of the GPR indices used for root biomass estimation is fully independent from root water content. Differentiating the contribution of root size and root water content on root radar signal will improve the accuracy of GPR-based root biomass estimation. Because of the difference in sensitivity to root water content variation between time interval index and signal-strength related indices, one possibility is to establish multiple regression models linking root size and root water content to different GPR indices. For example, based on a small amount of excavation, regression models between GPR indices extracted on radargrams and measured root biomass and root water content can be established:

$$dT = f(RB, RWC), \quad (3)$$

$$Pixels = f(RB, RWC), \quad (4)$$

where *RB* is root biomass, and *RWC* is root water content. The forms and parameters of regression models should be optimized based on site-specific conditions. Then, root biomass and root water content of any detected root can be solved by *dT* and *Pixels* extracted from its radar signal.

Another possible improvement is indirect prediction of root biomass by GPR, such as by converting the root fresh weight per unit area estimated by GPR into the root biomass with the root water content status of the survey area, or calculating root biomass from root diameters that are estimated by GPR. Moreover,

given the fact that the time interval index can be used to estimate both root biomass and fresh weight, water content of roots can be approximated (Table 6). Based on the estimated root fresh weight and root water content, the specific root biomass of each root reflector can be predicted.

Finally, up to now, all the GPR indices used for root quantification are extracted from the time domain. Developing new index in the frequency domain may be another approach to suppress the root water content's impact on root biomass estimation.

Conclusions

Both theoretical forward simulation and field controlled experiments conducted in this study confirmed the impact of root water content on root biomass estimation using GPR, and suggested that using the linear regression model between root biomass and radar reflectance related GPR index for root biomass estimation would only be feasible for roots possessing a narrow range of water content. Accuracy comparison among different estimation models indicated that the two new estimation models (one using the time interval index, Linear *dT* Model, and the other using non-linear regression, Non-linear *Pixels* Model) could increase root biomass estimation accuracy, especially for roots with greater root water content variability. For this reason, we suggest conducting a root water content investigation before beginning a root GPR survey. Appropriate GPR index and regression models can then be selected based on the water content range and orientation pattern of roots. Future efforts are needed to test the feasibility of the methods proposed in this study for discerning the effects of root size and root water content on root radar signal. Findings in this study can enhance the overall application of GPR for in situ root quantification.

Acknowledgments We thank Xin Cao, Ruyin Cao, Yuan Wu, Dameng Yin, Shengqiang Wang, Cong Wang, Yuhao Rao, and Jianmin Wang for their help during the field experiments. We thank Isaac Hopkins for his help in polishing the English of this paper. We also thank two anonymous reviewers for their comments to improve this paper. This study was supported by the National Natural Science Foundation of China (Grant No. 41001239), the Ph.D. Programs Foundation of the Ministry of Education of China and Open project supported by State Key Laboratory of Earth Surface Processes and Resource Ecology.

References

- al Hagrey SA (2007) Geophysical imaging of root-zone, trunk, and moisture heterogeneity. *J Exp Bot* 58:839–854. doi:10.1093/jxb/erl237
- Barton CVM, Montagu KD (2004) Detection of tree roots and determination of root diameters by ground penetrating radar under optimal conditions. *Tree Physiol* 24:1323–1331. doi:10.1093/treephys/24.12.1323
- Butnor JR, Doolittle JA, Kress L, Cohen S, Johnsen KH (2001) Use of ground-penetrating radar to study tree roots in the southeastern United States. *Tree Physiol* 21:1269–1278. doi:10.1093/treephys/21.17.1269
- Butnor JR, Doolittle JA, Johnsen KH, Samuelson L, Stokes T, Kress L (2003) Utility of ground-penetrating radar as a root biomass survey tool in forest systems. *Soil Sci Soc Am J* 67:1607–1615. doi:10.2136/sssaj2003.1607
- Butnor JR, Stover DB, Roth BE, Johnsen KH, Day FP, McInnis D (2008) Using ground-penetrating radar to estimate tree root mass comparing results from two Florida surveys. In: Allred BJ, Daniels JJ, Ehsani MR (eds) *Handbook of agricultural geophysics*. CRC Press, Boca Raton, pp 375–382
- Conyers LB (2004) *Ground-penetrating radar for archaeology*. AltaMira Press, Walnut Creek
- Cox KD, Scherm H, Serman N (2005) Ground-penetrating radar to detect and quantify residual root fragments following peach orchard clearing. *HortTechnology* 15:600–607
- Cui XH, Chen J, Shen JS, Cao X, Chen XH, Zhu XL (2011) Modeling tree root diameter and biomass by ground-penetrating radar. *Sci China Earth Sci* 54:711–719. doi:10.1007/s11430-010-4103-z
- Cui XH, Guo L, Chen J, Chen XH, Zhu XL (2012) Estimating tree-root biomass in different depths using ground-penetrating radar: evidence from a controlled experiment. *IEEE TGRS on-line first*. doi:10.1109/TGRS.2012.2224351
- Daniels DJ (2004) *Ground penetrating radar*, 2nd edn. Institution of Electrical Engineers, London
- Dannoura M, Hirano Y, Igarashi T, Ishii M, Aono K, Yamase K, Kanazawa Y (2008) Detection of *Cryptomeria japonica* roots with ground penetrating radar. *Plant Biosyst* 142:375–380. doi:10.1080/11263500802150951
- Forest Products Laboratory (1999) *Wood handbook-wood as an engineer material*. Gen. Tech. Rep. FPL-GTR-190. U.S. Department of Agriculture, Forest Service. Forest Products Laboratory, Madison, p 463
- Giannopoulos A (2005) Modelling ground penetrating radar by GprMax. *Constr Build Mater* 19:755–762. doi:10.1016/j.conbuildmat.2005.06.007
- Guo L, Chen J, Cui XH, Fan BH, Lin H (2013a) Application of ground penetrating radar for coarse root detection and quantification: a review. *Plant Soil* 362:1–23. doi:10.1007/s11104-012-1455-5
- Guo L, Lin H, Fan BH, Cui XH, Chen J (2013b) Forward simulation of root's ground penetrating radar diagram: Simulator development and validation. *Plant Soil*. (under review)
- Hirano Y, Dannoura M, Aono K, Igarashi T, Ishii M, Yamase K, Makita N, Kanazawa Y (2009) Limiting factors in the detection of tree roots using ground-penetrating radar. *Plant Soil* 319:15–24. doi:10.1007/s11104-008-9845-4
- Hirano Y, Yamamoto R, Dannoura M, Aono K, Igarashi T, Ishii M, Yamase K, Makita N, Kanazawa Y (2012) Detection frequency of *Pinus thunbergii* roots by ground-penetrating radar is related to root biomass. *Plant Soil* 360:363–373. doi:10.1007/s11104-012-1252-1
- Hruška J, Čermák J, Sustek S (1999) Mapping tree root systems with ground-penetrating radar. *Tree Physiol* 19:125–130. doi:10.1093/treephys/19.2.125
- Neto PX, de Medeiros WE (2006) A practical approach to correct attenuation effects in GPR data. *J Appl Geophys* 59:140–151. doi:10.1016/j.jappgeo.2005.09.002
- Oppenheim AV, Schaffer RW (1975) *Digital signal processing*. Prentice Hall, Englewood Cliffs
- Samuelson LJ, Butnor J, Maier C, Stokes TA, Johnsen K, Kane M (2008) Growth and physiology of loblolly pine in response to long-term resource management: defining growth potential in the southern United States. *Can J Forest Res* 38:721–732. doi:10.1139/x07-191
- Stover DB, Day FP, Butnor JR, Drake BG (2007) Effect of elevated CO₂ on coarse-root biomass in Florida scrub detected by ground-penetrating radar. *Ecol* 88:1328–1334. doi:10.1890/06-0989
- Straube J, Onysko D, Schumacher C (2002) Methodology and design of field experiments for monitoring the hygrothermal performance of wood frame enclosure. *J Build Phys* 26:123–151. doi:10.1177/0075424202026002098
- Su YZ, Li YL, Zhao HL (2006) Soil properties and their spatial pattern in a degraded sandy grassland under post-grazing restoration, Inner Mongolia, northern China. *Biogeochem* 79:297–314. doi:10.1007/s10533-005-5273-1
- Truss S, Grasmueck M, Vega S, Viggiano DA (2007) Imaging rainfall drainage within the Miami oolitic limestone using high-resolution time-lapse ground-penetrating radar. *Water Resour Res* 43. doi:10.1029/2005WR004395
- Turner G, Siggins AF (1994) Constant Q-attenuation of subsurface radar pulse. *Geophys* 59:1192–1200. doi:10.1190/1.1443677
- Yamanaka T, Kaihotsu I, Oyunbaatar D, Ganbold T (2007) Summertime soil hydrological cycle and surface energy balance on the Mongolian steppe. *J Arid Environ* 69:65–79. doi:10.1016/j.jaridenv.2006.09.003